scientific reports

Check for updates

OPEN

Telomere-related gene risk model predicts prognostic and immune microenvironment alterations in prostate cancer

Danfeng Zhao[1,4], Zhenjie Zang[1,2], Haodong Li[3], Ruiyu Li[3], Guanbo Wang[1,4], Keqin Zhang[1,4], Tongxiang Diao[1] & Qiang Fu[1,2,3,4]✉

The improvement of the prediction of prostate cancer (PCa) is a major challenge in disease management. This study analysed a total of 147,856 cells and identified 15 distinct cell types using single-cell RNA-sequencing (scRNA-seq) and bulk RNA-seq data from TCGA and GEO databases. Of these cells, 31,256 exhibited a high telomere-related gene score and were predominantly composed of myeloid dendritic cells (mDCs). Simultaneously, pseudo-temporal analysis indicated that mDCs are in the later stages of the differentiation trajectory, suggesting the significant role of mDCs as telomere-active cells in the development of PCa. Analysis of cell-cell communication revealed significant differences, particularly an increase in communication between mDCs and CTLs, alongside a decrease in communication between mDCs and B cells. These variations may represent critical nodes influencing the development of PCa. Additionally, two hub genes were utilized to create risk models, with ROC curves confirming their predictive efficacy for 3-, 5-, and 10-year survival rates in patients. Functional analysis of these genes was conducted, and NPY siRNA transfection notably inhibited proliferation in LNCaP and DU145 cells. Furthermore, the models demonstrated that high-risk patients had poorer overall survival, greater immune infiltration, and reduced sensitivity to chemotherapeutic drugs.

Keywords Prostate cancer, Single-cell RNA-sequencing, Telomere-related gene, Risk mode, Tumour immune environment

Among men in Western countries, prostate cancer (PCa) is the most prevalent malignant tumour of the urinary tract and the second leading cause of cancer-related deaths[1]. According to a study published in CA: A Cancer Journal for Clinicians, there are approximately 280,000 new cases of PCa in the United States each year, which results in more than 30,000 deaths[2]. Despite the typically slow growth of PCa, patients with high-risk cancers often have poor outcomes even after aggressive treatments such as surgery, hormone therapy, and immunotherapy[3]. Hence, the identification of new potential molecular biomarkers for targeted treatment and prognostic evaluation of PCa patients are crucial.

Telomeres consist of GT-rich DNA repeat sequences that play crucial roles in protecting and preventing chromosome ends from being recognized as DNA damage sites[4]. With each cell proliferation, telomeres progressively shorten, thus leading to cellular senescence and eventual death[5]. In many tumours, telomeres are maintained through the upregulation of telomerase, which enables cells to continuously divide, proliferate, and avoid immune surveillance[6]. There is growing evidence indicating that telomeres play a crucial role in the biology of immune cells, including T cells[7]. Numerous studies have consistently shown that dendritic cells (DCs) are the most effective antigen-presenting cells in the immune system and can infiltrate tumour sites[8]. In a stable state, DCs display self-antigens to T cells, thus leading to the development of immune tolerance and tumour progression[9]. Hence, it is imperative to gain a comprehensive understanding of the role of telomere-related (TR) genes in the immune mechanisms involved in the progression of PCa.

Single-cell RNA sequencing (scRNA-seq) integrated with bulk RNA-seq represents an advanced bioinformatics approach that enables the identification of novel molecular biomarkers and facilitates the

[1]Department of Urology, Shandong Provincial Hospital, Shandong First Medical University, Jinan 250021, Shandong, China. [2]College of First Clinical Medicine, Shandong University of Traditional Chinese Medicine, Jinan 250199, China. [3]Department of Urology, Shandong Provincial Hospital, Shandong University, Jinan 250021, Shandong, China. [4]Engineering Laboratory of Urinary Organ and Functional Reconstruction, Shandong Provincial Hospital, Shandong First Medical University, Jinan 250021, Shandong, China. ✉email: fuqiang@sdfmu.edu.cn

construction of prognostic models with non-invasive potential. Recent studies have identified HEATR5B, DDC, and WHSC1 as potential biomarkers for PCa, capable of predicting the malignant progression of the disease[10,11]. Furthermore, Luis Rueda et al. developed predictive models that can effectively distinguish specific Gleason scores, offering a novel theoretical basis for simplifying the assessment of Gleason scores[12]. In this study, we conducted a comprehensive bioinformatics analysis to investigate genes associated with telomeres in PCa. Our objective was to elucidate the significant roles of these genes in the development of tumours. Additionally, we constructed a prognostic model specifically for PCa patients and evaluated its effectiveness in stratifying risk. Furthermore, we conducted a comprehensive analysis to investigate the relationship between risk models and infiltrating immune cells to gain a better understanding of the immune processes involved in the progression of PCa.

Materials and methods

Acquisition of transcriptome data

Data from various publicly available sources, including The Cancer Genome Atlas (TCGA, https://portal.gdc.cancer.gov/) and the Gene Expression Omnibus (GEO, https://www.ncbi.nlm.nih.gov/geo/) were used in this study. The TCGA-PRAD dataset ($n = 554$) consisted of 502 tumour samples and 52 adjacent samples, with survival information available for 418 PCa tumour samples. The GSE21032-GPL5188 dataset (150 tumour samples and 29 normal samples), which included 117 PCa tumour samples with survival information, was included in this study. Throughout this study, the data access policies of each database were respected.

Analysis of scRNA-seq data

In this study, we obtained scRNA-seq data for PCa from the GEO database (GSE181294). A total of 37 samples were selected, including 18 tumor samples, 14 healthy samples, and 5 normal samples. The GSE181294 data were imported into the "Seurat" package and included a total of 157,824 cells, with an average of 4,042 cells per sample[13]. This study applied several criteria to filter out low-quality cells and genes. (1) Cells expressing fewer than 200 genes were excluded from the analysis. (2) Genes expressed in less than 1 cell were excluded from the analysis. (3) Cells with between 200 and 7000 expressed genes were retained in the analysis. (4) Cells retaining less than 1% of red blood cell genes were retained in the analysis. (5) Cells with UMI readings greater than 600 were retained in the analysis. A total of 157,290 cells were obtained via filtration, followed by removal of doublets, thus resulting in 147,856 cells. Genes with high variability were identified by normalizing the data using the "normalizedata" function in the Seurat R package. Subsequently, we utilized significant principal components (PCs) to cluster the data by using a graph-based PCA approach. The harmony method was used to remove batch effects between different samples. The "FindClusters" function was used for clustering, thus resulting in 19 clusters at a resolution of 0.8 on 15 PC components. Subsequently, the "RunUMAP" function was used for uniform manifold approximation and projection (UMAP) to explore cell clustering via UMAP-1 and UMAP-2. To identify differentially expressed genes (DEGs) in each cell cluster, we utilized normalized gene expression data and the Seurat "FindAllMarkers" function. After identifying cell clusters by using specific biomarkers for each cell type, the proportions of cell types were calculated and evaluated by annotating the marker genes of the cells.

TR gene scores

TR gene scores were calculated by using the R package "AUCell" through gene set enrichment analysis. We scored 212 selected TR genes based on their areas under the curves by referring to the CancerTelSys database (http://www.cancertelsys.org/telnet/). This gene expression ranking of each cell allows us to estimate the proportion of highly expressed genes in each cell. To identify cells with an active gene set, the "AUCell_exploreThresholds" function was used. The AUC of each cell was subsequently visualized via UMAP embedding by using the "ggplot2" R package to represent the activated cell clusters.

Trajectory analysis

Trajectory analysis was performed by using the "Monocle 2" package. This package generates a pseudotime trajectory by employing reverse graph embedding and a user-defined gene list[14]. This allows for the interpretation of branching and linear differentiation processes. For the trajectory analysis of TR cell populations, the raw count data were normalized by using estimated trajectory inference size factors. Pseudotime trajectories were constructed by using highly variable and highly expressed genes (discrete estimate ≥ 1 and average expression ≥ 0.1)[15]. The default parameters were selected for the "DDRTree" algorithm. We used Monocle 2 to analyse gene expression in branch-separated cells[14]. A heatmap of branch-dependent expression patterns was generated by using Monocle 2.

Cell–cell communication analysis

The CellChat dataset was created by using the "CellChat" package, which utilized UMI count matrices for each group (PCa and normal)[16]. The analysis of cell-cell communication was performed by using the CellChatDB human ligand–receptor interaction database as a reference. The "mergeCellChat" function was used to combine CellChat objects for each group, thus allowing for comparisons of interaction counts and strengths. To visualize the differences in interaction counts or strengths between different cell types among the groups, the "netVisual_diffInteraction" function was used. Additionally, the distribution of signal gene expression between groups was visualized by using the "netVisual_bubble" and "netVisual_aggregate" functions.

Gene ontology (GO) and Kyoto encyclopedia of genes and genomes (KEGG) pathway enrichment analysis

GO enrichment analysis involved analyses of biological processes (BP), molecular functions (MF), and cellular components (CC)[17]. KEGG is a bioinformatics resource that facilitates the investigation of metabolic pathways that are altered in gene lists[18]. To analyse DEGs associated with telomeres in PCa, the "clusterProfiler" package was utilized for GO and KEGG enrichment analyses[19–21].

Construction and validation of prognostic models

Univariate Cox regression analysis was also conducted to evaluate the correlation between each telomere-related DEG (TRDEG) and overall survival (OS) in the tumour cohort. Genes with a P value < 0.05 were considered to be significantly associated with OS and were further analysed. The tumour samples with clinical information were randomly divided into a training set ($n = 351$) and a validation set ($n = 184$). To further specify candidate genes and construct the prognostic model, we performed least absolute shrinkage and selection operator (LASSO) Cox regression by using the "glmnet" package[22]. The penalty parameter (λ) was determined based on the minimum standard. The following formula was used to calculate the risk score:

$$RiskScore = \sum_{i=1}^{n} Coef\left(gene_i\right) * Expression\left(gene_i\right)$$

(Coef ($gene_i$): risk factor; Expression ($gene_i$): gene expression level)

To evaluate the prognostic value of the training set, the samples were divided into two groups based on the median risk score. Survival curves were plotted by using Kaplan–Meier analysis, and statistical significance was determined by using the log-rank test. The performance of the prognostic model was validated by using receiver operating characteristic (ROC) curves. The area under the curve (AUC), which ranges between 0.5 and 1, indicates the model's performance, with a higher value indicating better performance. Similarly, the patients in the validation set were also divided into high- and low-risk groups to validate the risk score model.

Construction and validation of the nomogram

Clinical data, including age, TNM stage, and pathological stage, were extracted from the TCGA and GEO cohorts. Clinical information was incorporated into a prognostic model to conduct univariate Cox regressions and multivariate Cox regressions. Furthermore, a nomogram was generated with the "RMS" package, which integrates prognostic and clinical features to predict OS at 3-, 5-, and 10-year intervals. The performance of the nomogram was assessed by using time-dependent ROC curves.

Cell culture

The human PCa cell lines were obtained from Procel (Procell Life Science & Technology, Wuhan, China). 22RV1, DU145, and LNCaP cells were cultured in MEM and RPMI 1640 medium supplemented with 10% FBS. The RWPE-1 cell line was cultured in K-SFM.

Cell transfection

Transfection of small interfering RNA (siRNA) from General Biol (Anhui, China) into cell lines was conducted by using Lipofectamine 2000 (Invitrogen in CA, USA). The transfection medium was changed to complete medium supplemented with 10% FBS after 6 h, and the cells were incubated for 24–48 h. The sequences of siRNAs are listed in Supplementary Table S1.

Protein and mRNA expression analysis

The protein data of human tissue were downloaded from The Human Protein Atlas (HPA, https://www.proteinatlas.org/). Total RNA was extracted with TRIzol reagent following quantitative real-time PCR (qRT-PCR). cDNA was obtained by incubating 1 μg of RNA with PrimeScript RT Master Mix. Quantitative real-time polymerase chain reaction was performed in triplicate by using the Roche LightCycler 480 real-time PCR System. The relative expression level was calculated by using the 2-ΔΔCt method. The PCR primers used are listed in Supplementary Table S2.

Cell proliferation assays

A Cell Counting Kit-8 (CCK-8) assay was used to measure cell proliferation. A total of 3000 cells were seeded per well in 96-well plates. A 10% CCK-8 solution in 100 μL of fresh medium was used to replace the culture medium, and the plates were incubated for 1 h. Microplate readers were used to measure cell proliferation by measuring the absorbance of the wells at 450 nm.

Gene set enrichment analysis (GSEA) and gene set variation analysis (GSVA) enrichment analysis

GSEA is a method used to identify statistically significant consistent differences in gene expression between two biological states by using a predefined set of genes[23]. In this study, we utilized the "clusterProfiler" package to analyse an ordered list of genes based on log2-fold change values with 1000 gene set permutations performed for each analysis. The reference gene set that was used in our analysis was "c2.cp.kegg.v7.5.1.symbols" from the Molecular Signatures Database (MSigDB). To investigate the biological functional differences between the PCa and control groups, GSVA was performed with the R package "GSVA" based on "c2.cp.kegg.v7.5.1.symbols"[24]. The GSVA method was used to calculate the gene set scores for each sample. The minimum and maximum limits for the number of genes in a single gene set were set at 2 and 10,000, respectively. Additionally, the percentile of

each gene set score in each sample was set to 1. A gene set with a P value < 0.05 was considered to be significantly enriched. The results were visualized by using the "pheatmap" function.

Immune microenvironment analysis

In single-sample gene set enrichment analysis (ssGSEA), enrichment scores are calculated separately for the samples and gene sets[25]. The ssGSEA enrichment score represents the degree of coordinated up- or downregulation of genes in a specific gene set within the sample. According to the Tumour and Immune System International (TISIDB, http://cis.hku.hk/TISIDB/index.php) database, 28 immune cell types were analysed to calculate the relative enrichment scores of each immune cell, and the "ggplot2" package was used to visualize the differences between the two groups[26].

Tumour mutation burden (TMB) and chemotherapy sensitivity analysis

The landscape of genomic mutational variation is illustrated by using mutation data. The R package "maftools" was used to visualize somatic variants across different clusters. Generally, frequently mutated genes with the highest 20 mutation frequencies are regarded as being the primary driver genes for malignant tumours[27,28]. The R package "oncoPredict" was used to predict potential therapeutic drug susceptibilities of patients in high- and low-risk groups of PCa. The data obtained from the Genomics of Drug Sensitivity in Cancer (GDSC, https://www.cancerrxgene.org/) database included data on half-maximal inhibitory concentrations and gene expression[29,30].

Statistical analysis

The relationships between two groups of continuous variables were examined by using the nonparametric Wilcoxon rank sum test. Comparisons between proportions were evaluated by using either the chi-square test or Fisher's test. The log-rank test was used to evaluate significant differences between the Kaplan–Meier survival curves generated by the "ggsurvplot" function of the "survminer" package. LASSO Cox regression analyses were also conducted to screen and construct a model of the characterized genes, and the predictive performance of the genes was assessed by using ROC and time-dependent ROC curves. Differences were considered to be statistically significant when a two-sided P > 0.05 was used. R software (version 4.1.2) was used for all of the analyses, and the Benjamini–Hochberg method was utilized to adjust the P values. **** P < 0.0001, *** P < 0.001, ** P < 0.01, * P < 0.05.

Results

Cell cluster constitution of PCa

Figure 1 shows the flowchart of this study. To investigate the sources of the highly expressed genes, we analysed of cell clusters in PCa by using an scRNA-seq dataset (GSE181294). After performing initial quality control and removing doublets, we obtained a total of 147,856 cells from the single-cell transcriptome. This study included 37 samples, including PCa and normal tissues. The distribution of cells among these three groups was relatively even, thus indicating the absence of significant batch effects between samples and enabling subsequent analysis. Afterwards, all of the cells were grouped into 19 clusters, and the gene expression characteristics of each cluster were used to annotate different cell types by using cell-specific biomarkers (Fig. 2). Figure 2D illustrates the identification of 15 cell types, including CTL, Treg, and Thelper, and the proportions of different cell types in each group are presented. Dot plots were generated to visualize the specific genes associated with each cell type (Fig. 2E).

Calculation of TR gene scores

Based on various annotated cell types, we attempt to find the cell type with higher telomerase activity. The identification of the cell set with a high TR gene score was conducted by analysing the expression pattern of TR genes at the single-cell level. By determining the optimal threshold, a total of 31,256 cells were identified as the high TR gene score set (Supplementary Figure S1A). The distribution of the cell sets were shown in the UMAP plot in Supplementary Figure S1B. Cell clusters with an AUC greater than 0.17 were considered to be part of the high TR gene score set and were mainly composed of mDC.

Trajectory analysis

Subsequently, we conducted pseudo-temporal analysis on all telomere active cells to evaluate the distribution of mDCs in the differentiation trajectory. The pseudotime cell trajectory was established by selecting all of the cells with an AUC above a certain threshold, thus allowing us to identify the underlying gene expression program that drives the progression of PCa. The transcriptional states along the trajectory demonstrated distinct processes. At the initial part of the trajectory, we found endothelial cells, epithelial cells, and pericytes, whereas macrophages, mast cells, mDCs, and monocytes were positioned at the end of the trajectory. CTL, Thelper, and Treg cells were in the transitional stage (Figs. 3A-D). To understand the molecular basis of this transformation, we examined the genes involved in the branching of PCa cells. The genes that were highly expressed in the prebranch region were mainly enriched in GO biological process terms such as focal adhesion and cell leading edge. Genes that were highly expressed in cell branch 1 were enriched in the pathways of T-cell activation and mononuclear cell differentiation. The genes that were highly expressed in cell branch 2 were mainly enriched in the pathways of antigen processing and the presentation of exogenous antigen, as well as in the pathways of the presentation of peptide antigen via MHC class II (Fig. 3E).

Cell–cell communication analysis

Exploring the cell-cell interaction network in the PCa tumor microenvironment (TME), especially with mDCs as the initiator or receiver of communication, and the significantly altered communication signals between PCa

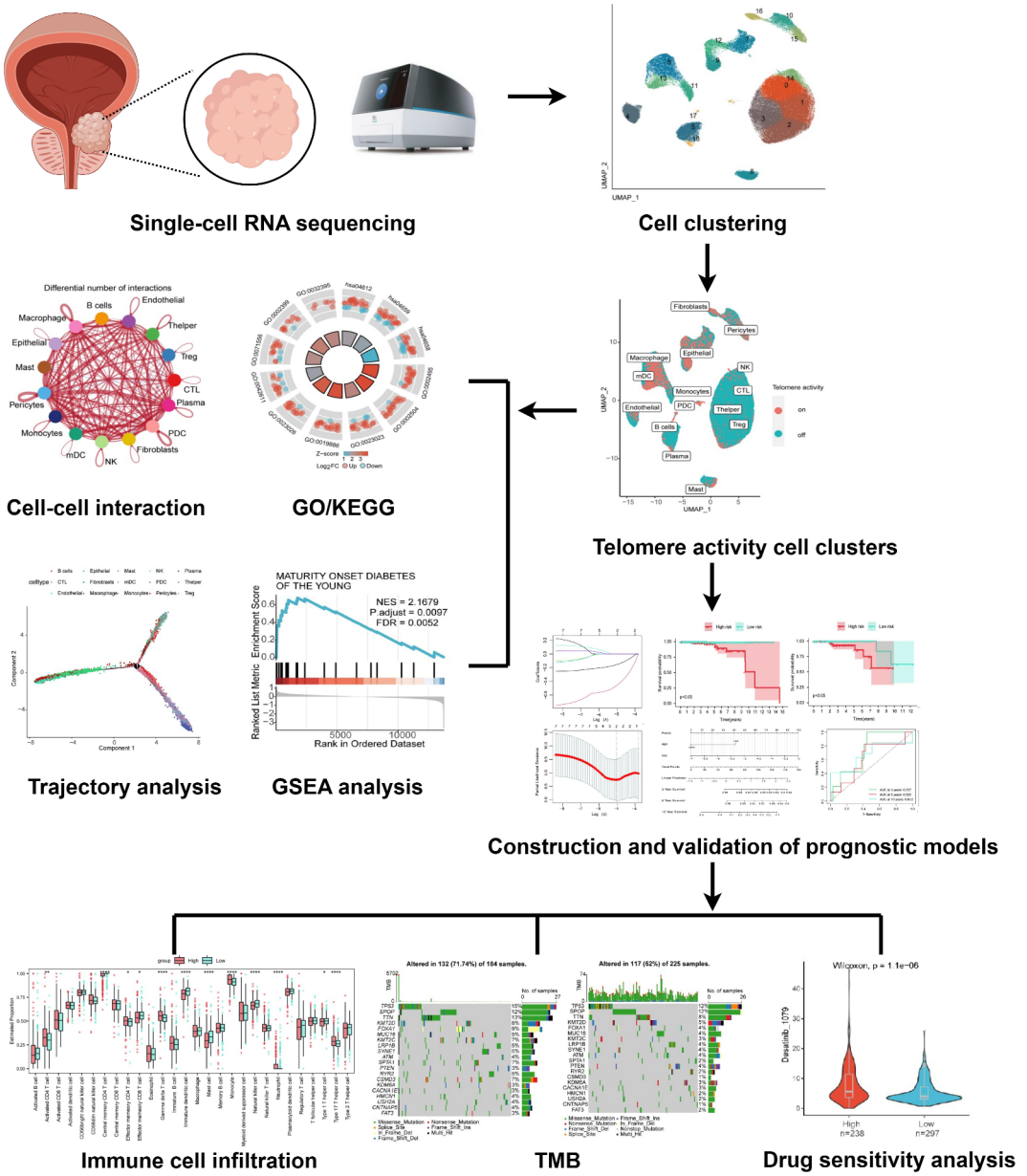

Fig. 1. Working flow of the research.

and the control group, can further explain how mDCs with the highest telomere activity affect the progression of PCa patients. Therefore, we utilized the R package "CellChat" to examine the changes in cell crosstalk between normal tissue and PCa tissue. We observed that the number and strength of interactions among PCa tissues were greater than those among normal tissues (Fig. 4A). Specifically, interactions among immune cells increased both the number and strength of immune cells (Fig. 4B). It is evident from these findings that the microenvironment of the immune system is complex. The patterns of signal reception and transmission between normal tissue and PCa tissue are clearly depicted in Figs. 4C and D. Notably, in cancer tissue, the MIF signalling pathway received by B cells is weakened. To explore key TR genes, we focused on mDCs. Furthermore, we analysed receptor–ligand pairs that potentially regulate communication between mDCs and other immune cells. The interaction between HLA-C ligands derived from mDCs and their corresponding receptors on CTLs is increased in PCa (Supplementary Figs. 2 A). Conversely, the interaction between MIF ligands derived from mDC and their corresponding receptors on B cells is decreased in PCa (Supplementary Figs. 2B). We further investigated the interaction between the MHC-I and MIF pathways in PCa cells. We observed no significant change in the expression level of ligands in the MHC-I signalling pathway in mDCs compared to that in the control cells, and the expression level of receptors in CTLs were increased. Additionally, the expression level of MIF ligands on mDCs were significantly decreased in PCa, whereas the expression of receptors on B cells was not significantly altered, thus explaining the weakened extent of the interaction between the MIF pathway and mDCs and B cells in PCa tissues (Supplementary Figs. 3).

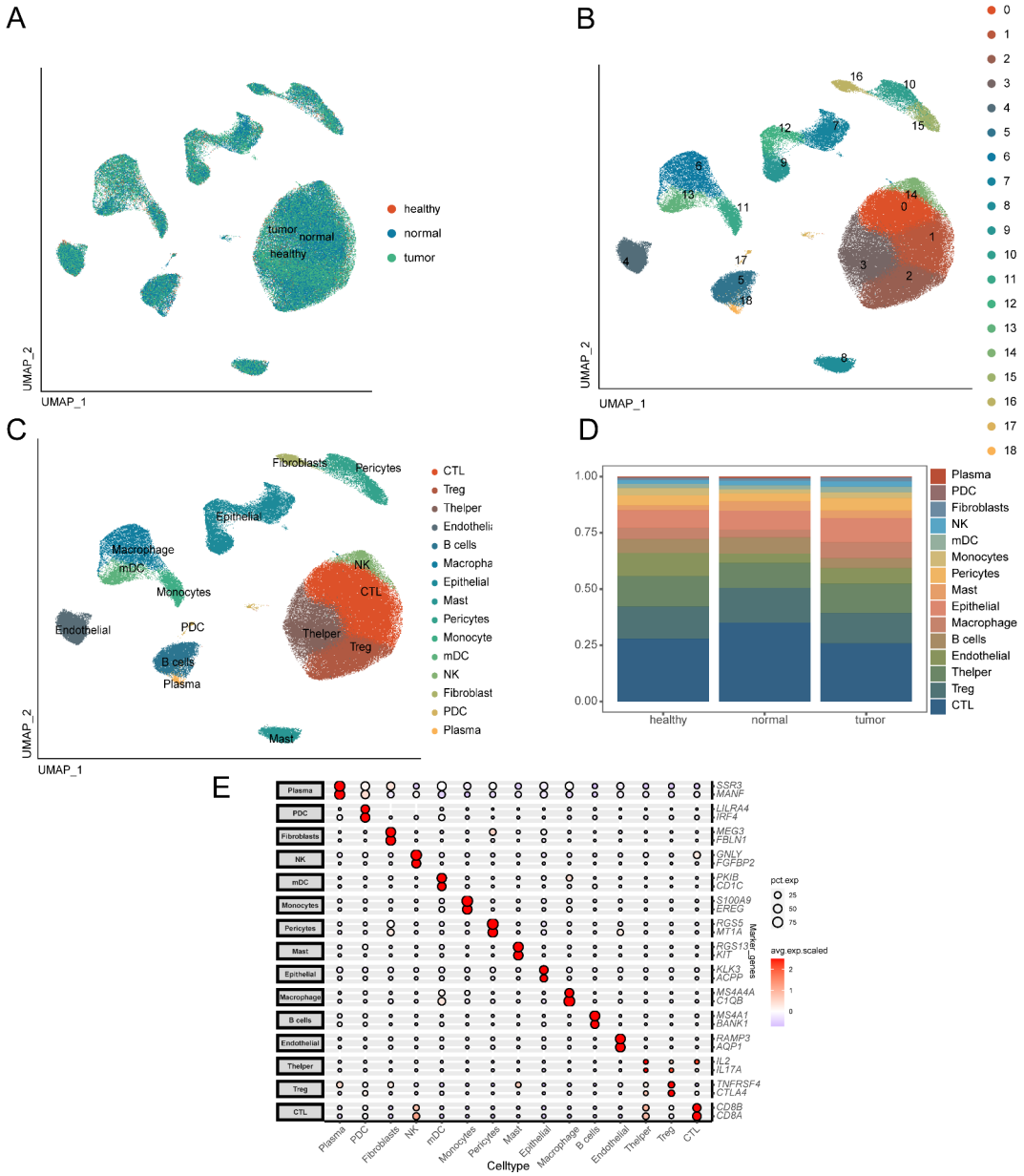

Fig. 2. Analysis of scRNA-sequencing data to identify cell subpopulations. (**A**) UMAP plot illustrating the distribution of different tissues. (**B**) UMAP plot illustrating the distribution of 18 cell clusters. (**C**) Cell types were identified based on marker genes. (**D**) Histogram showing the distribution of cell types in different tissues. (**E**) Marker gene expression levels in each cell cluster.

Enrichment analysis of TRDGEs

Furthermore, we combine single-cell and transcriptome research to identify the core targets of telomere-related genes that affect the progression of PCa. In PCa, a total of 13,772 DEGs were identified compared to those in normal tissues. These genes exhibited significant differences between the two groups (adjusted $P < 0.05$, |log2-fold change| > 0.5). The top 5 upregulated genes (PCA3, TRIM36, CAMKK2, CGREF1and RAB17) and the top 5 downregulated genes (AOX1, GPRC5B, MEIS2, CLU and PPP1R3C) in PCa are displayed in a heatmap (Fig. 5A). There were 1,063 DEGs between the TR activity and inactivity cell sets (adjusted $P < 0.05$, |log2-fold change| > 0.25; Fig. 5B).

To investigate the biological functions of these TRDEGs, we performed GO and KEGG enrichment analyses. GO analysis revealed enrichment of genes in the BP category, such as genes involved in antigen processing and the presentation of exogenous peptide antigens via MHC class II, antigen processing and the presentation of peptide antigens via MHC class II, and antigen processing and the presentation of peptide or polysaccharide antigens via MHC class II. In terms of CCs, the hub genes were enriched in the MHC class II protein complex, the MHC protein complex, and the integral component of the luminal side of the endoplasmic reticulum membrane. The hub genes were also enriched in the MFs of MHC class II protein complex binding, MHC protein complex

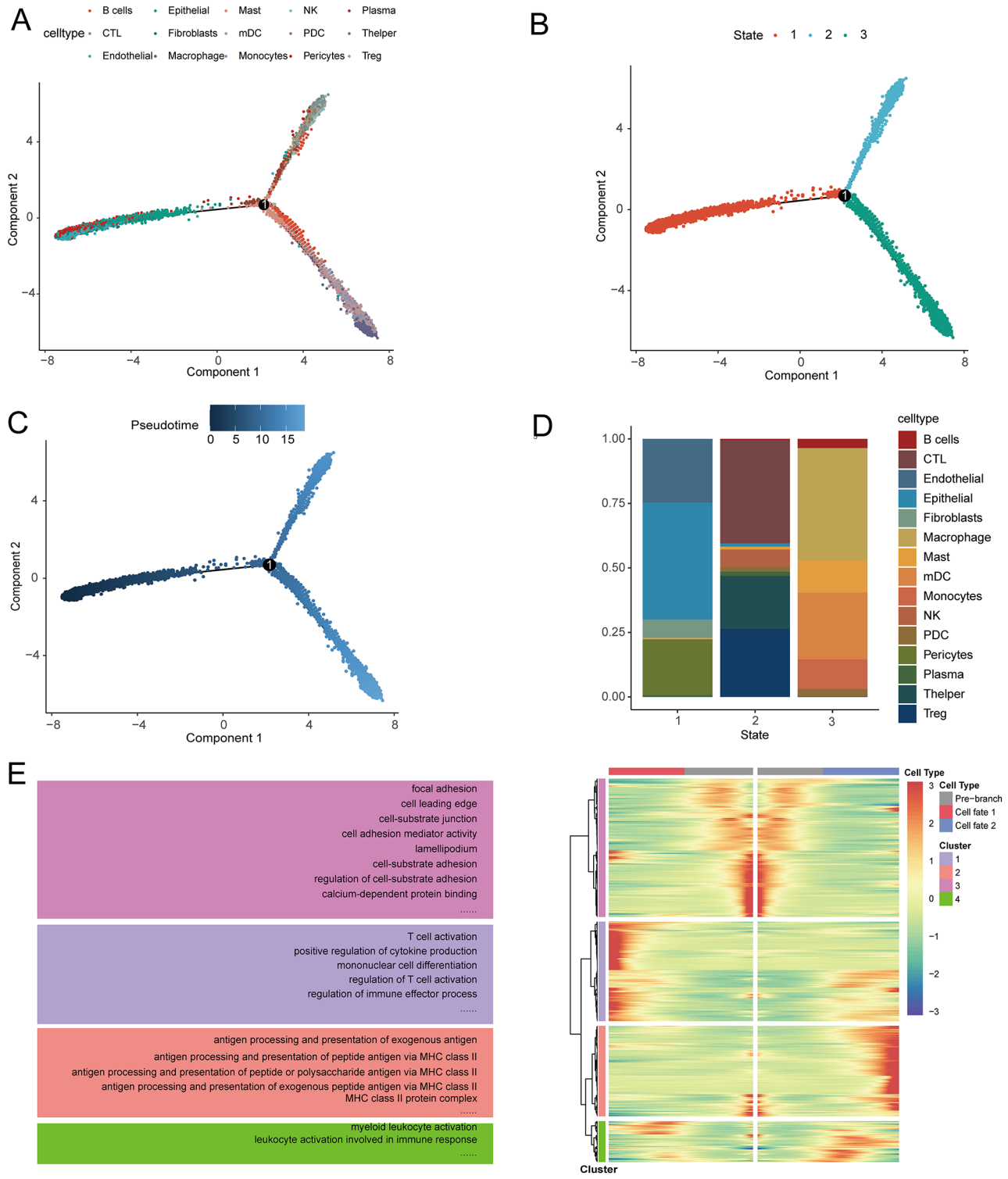

Fig. 3. Trajectory analysis demonstrates all of the cell transcriptional patterns with AUCs surpassing the threshold. (**A**) Trajectory analysis showing the distribution of PCa cells based on cell type. (**B**) The trajectory plot was classified into three distinct states by Monocle2. (**C**) The trajectory shows the cell developmental time in PCa. (**D**) The stacked bar plot displays the distribution of cell types in different states. (**E**) The heatmap illustrates DEGs among different branches. Enriched GO terms of different gene clusters in the heatmap are displayed on the left.

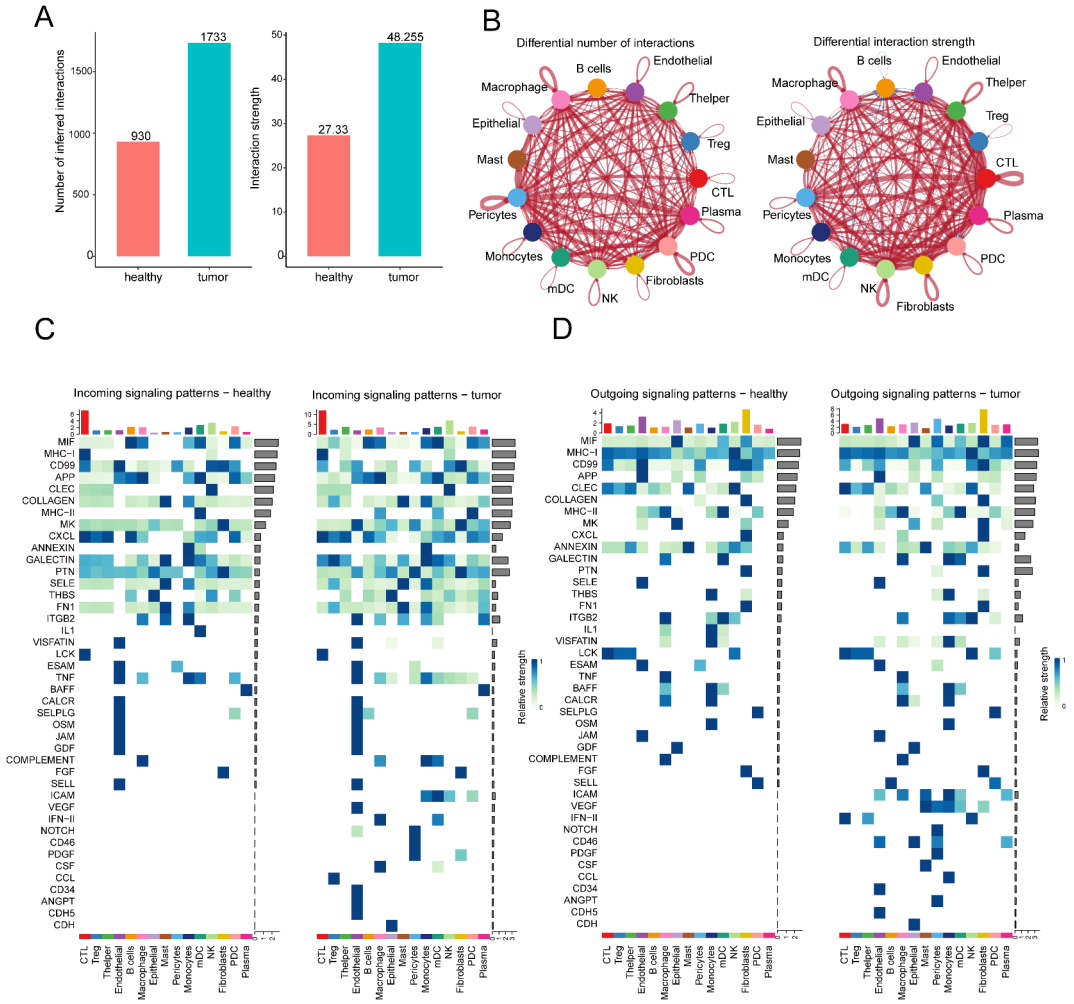

Fig. 4. Cell–cell communication interactions in normal and prostate cancer cells. (**A**) The bar chart illustrates the number and interaction strength of cell-cell communication interactions between normal and PCa cell types. (**B**) Network plots showing the number and interaction strength of cell-cell communication interactions between normal and PCa cell types. (**C**-**D**) Heatmap plots showing the incoming and outgoing signalling patterns in normal and PCa cell types.

binding, and MHC class II receptor activity. KEGG enrichment analysis demonstrated significant enrichment of pathways related to Th17 cell differentiation, Th1 and Th2 cell differentiation, and antigen processing and presentation (Fig. 5C). We then further analysed and clarified the core targets by intersecting the two sets (DEGs and TRDEGs), thus resulting in the identification of 249 hub genes (Fig. 5D).

Construction and validation of prognostic models

Based on the identified intersecting genes, we attempt to screen genes that significantly affect the prognosis of PCa patients and construct a prognostic model for patients. A total of 249 hub genes were used to identify cancer-related feature genes via univariate Cox analysis. Among these genes, 7 were found to be significantly associated with PCa prognosis. A random sampling method was used to select 7/10 of the PCa samples ($n = 535$) as the training set ($n = 351$), and the remaining 3/10 samples were used as the validation set ($n = 184$). LASSO regression analysis was performed on the training set, and 2 genes associated with PCa patient prognosis were identified, as shown in Figs. 6A and B. Based on the median risk value as the threshold, we divided the samples into high- and low-risk groups to assess the robustness of the model that was constructed by using these genes. Kaplan–Meier survival curves were constructed for different groups of patients in the training cohort (Fig. 6C) and validation cohort (Fig. 6D). The results showed that patients in the high-risk group had a significantly worse prognosis than patients in the low-risk group. ROC curves were used to evaluate the predictive performance of the risk model in terms of patient prognosis. In the training cohort, the AUC values for 3-, 5-, and 10-year survival were 0.974, 0.706, and 0.860, respectively (Fig. 6E). In the validation cohort, the AUC values for 3-, 5-, and 10-year survival were 0.886, 0.872, and 0.672, respectively (Fig. 6F). In addition, we conducted qRT-PCR experiments to analyse the expression levels of CSRP1 and NPY in tumour (22RV1, LNCaP, and DU145) and normal (RWPE-1) cell lines. Our findings demonstrated that the expression level of CSRP1 in RWPE-1 cells was significantly greater than that in tumour cell lines (Figs. 7A and C). Conversely, the expression of NPY showed

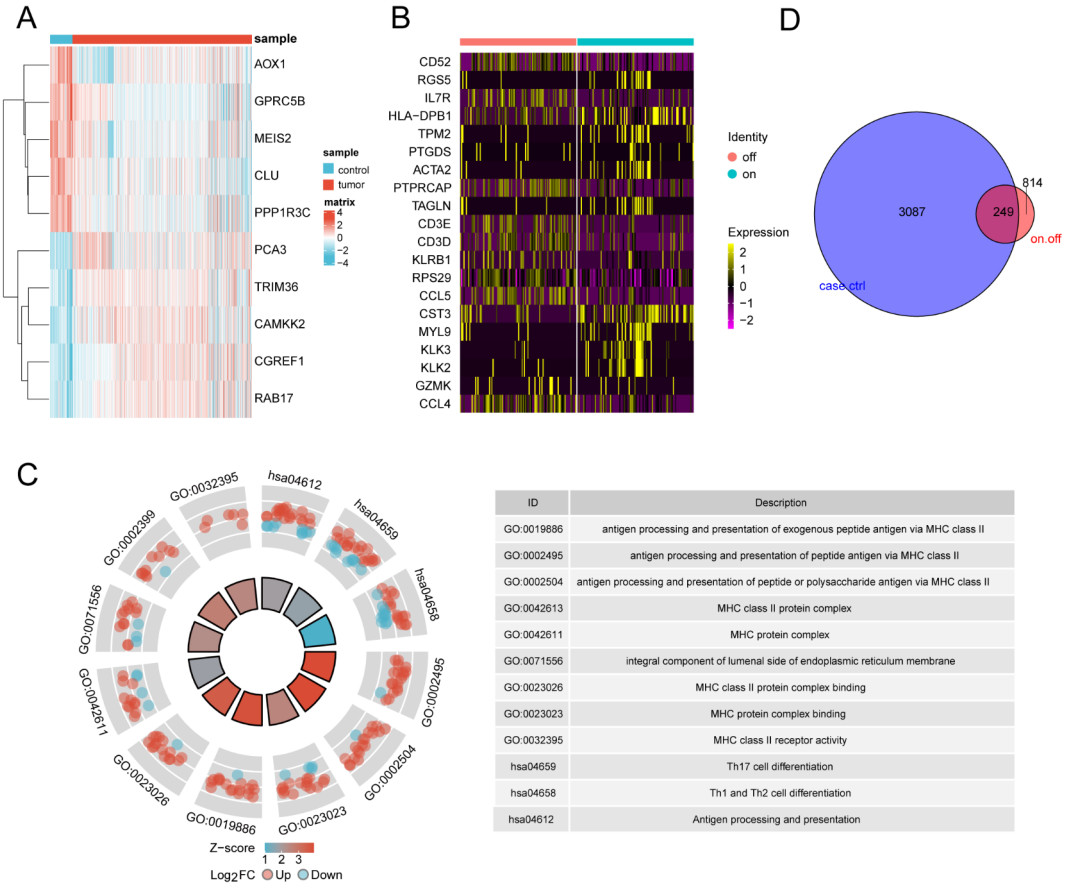

ID	Description
GO:0019886	antigen processing and presentation of exogenous peptide antigen via MHC class II
GO:0002495	antigen processing and presentation of peptide antigen via MHC class II
GO:0002504	antigen processing and presentation of peptide or polysaccharide antigen via MHC class II
GO:0042613	MHC class II protein complex
GO:0042611	MHC protein complex
GO:0071556	integral component of lumenal side of endoplasmic reticulum membrane
GO:0023026	MHC class II protein complex binding
GO:0023023	MHC protein complex binding
GO:0032395	MHC class II receptor activity
hsa04659	Th17 cell differentiation
hsa04658	Th1 and Th2 cell differentiation
hsa04612	Antigen processing and presentation

Fig. 5. Identification of TR genes with functional enrichment. (**A**) The heatmap shows the top 20 significant DEGs. (**B**) Heatmap showing the DEGs related of telomere activity in PCa cells. (**C**) Circle plot showing GO terms and KEGG pathway enrichment of TRDEGs. (**D**) Venn diagram showing the key genes between the groups.

the opposite pattern (Figs. 7B and D). Based on these results, we further evaluated cell proliferation by using the CCK-8 assay. We observed a significant decrease in the number of viable LNCaP and DU145 cells upon NPY knockdown (Figs. 7E-F). However, proliferation of 22RV1 cells was enhanced after CSRP1 knockdown (Figure S4).

GSEA and GSVA

To further investigate the potential mechanisms of the differentially expressed genes, we conducted GSEA. We utilized pathway information from the MsigDB database as a reference and identified the most significant pathways based on the NES. The GSEA results demonstrated significant enrichment of OLFACTORY TRANSDUCTION (NES = 2.6433, adjusted P = 0.0134, FDR = 0.0071), MATURITY ONSET DIABETES OF THE YOUNG (NES = 2.1679, adjusted P = 0.0097, FDR = 0.0052), HYPERTROPHIC CARDIOMYOPATHY HCM (NES = -2.5881, adjusted P = 0.0086, FDR = 0.0046), DILATED CARDIOMYOPATHY (NES = -2.6498, adjusted P = 0.0086, FDR = 0.0046), PENTOSE AND GLUCURONATE INTERCONVERSIONS (NES = 2.0491, adjusted P = 0.0098, FDR = 0.0052), and ARRHYTHMOGENIC VENTRICULAR CARDIOMYOPATHY ARVC (NES = -2.5624, adjusted P = 0.0086, FDR = 0.0046) in PCa (Supplementary Figure S5A). Additionally, we performed GSVA by using pathway information from the MsigDB as a reference. We selected several pathways that exhibited the most significant differences between the high- and low-risk groups and generated a heatmap (Supplementary Figure S5B).

Immune cell infiltration analysis

Further studies were conducted on 28 types of immune cells infiltrating high-risk and low-risk patients by using the ssGSEA method. Significant differences were observed between the high- and low-risk groups for most immune cell types, such as activated CD4 + T cells and central memory CD4 + T cells (Supplementary Figure S6A). There were positive correlations observed among most immune cell types, whereas a few showed negative correlations. For instance, activated CD8 + T cells exhibited a negative correlation with T follicular helper cells and memory B cells (Supplementary Figure S6B). Furthermore, significant correlations were observed between each intersecting gene and its corresponding immune cell type. The CSRP1 gene was significantly negatively correlated with activated CD4 + T cells (R = -0.3283, P < 0.001), monocytes (R = -0.4161, P < 0.001), and gamma

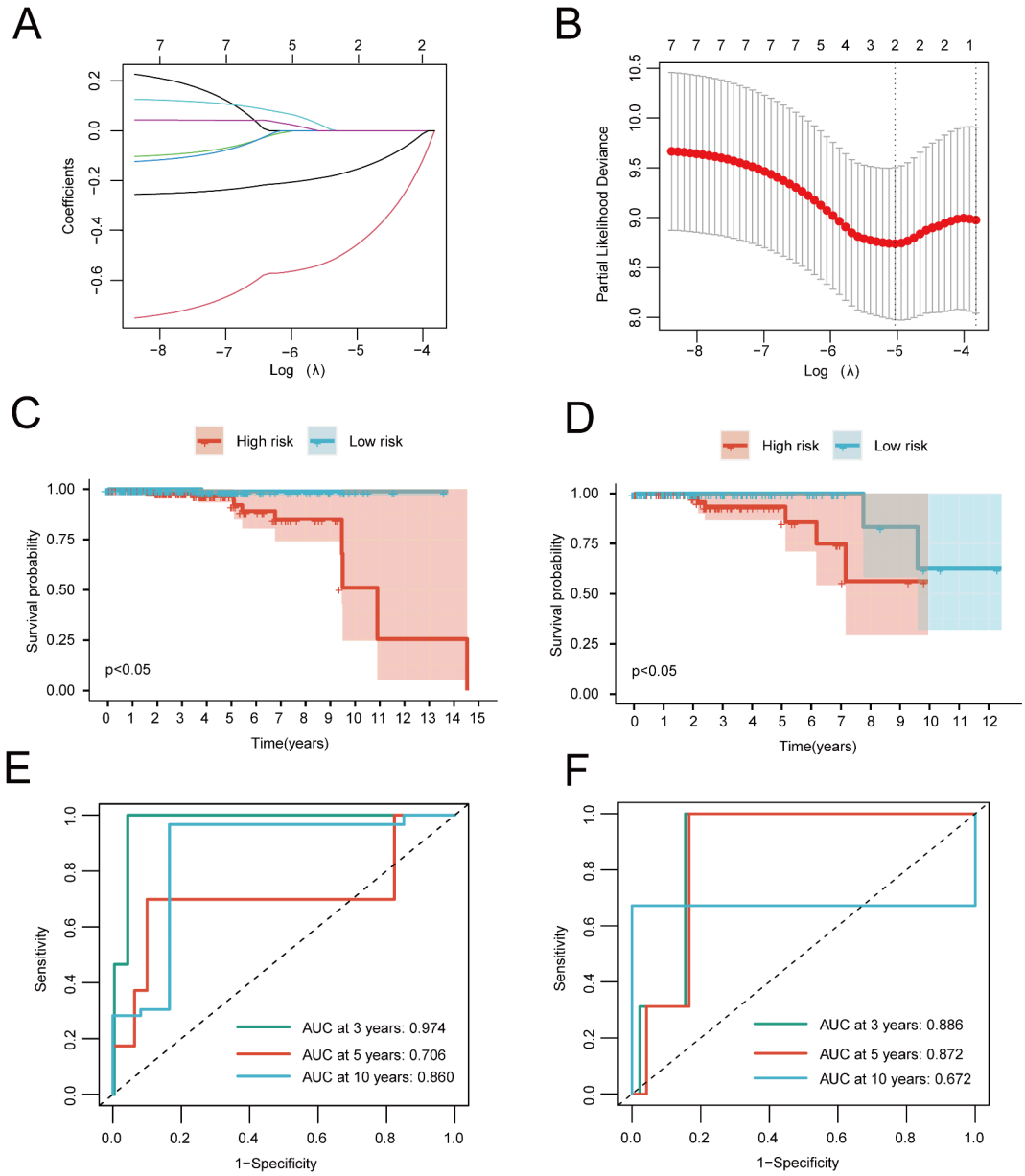

Fig. 6. Utilized hub genes from PCa samples to develop a risk model. (**A**-**B**) Gene selection by using LASSO regression analysis. (**C**-**D**) Risk score distribution and OS in the training and validation cohorts. (**E**-**F**) ROC curve analysis was performed to predict the risk of death in the training and validation cohorts.

delta T cells (R = -0.2903, P < 0.001) (Supplementary Figures S7A-C). Moreover, the expression of the CSRP1 gene was significantly positively correlated with the infiltration of type 1 T helper cells (R = 0.3109, P < 0.001), central memory CD4 + T cells (R = 0.4519, P < 0.001), natural killer cells (R = 0.2921, P < 0.001), and mast cells (R = 0.3289, P < 0.001) (Supplementary Figures S7D-F, H). Additionally, the NPY gene exhibited significant positive correlations with monocytes (R = 0.2369, P < 0.001) and immature dendritic cells (R = 0.2742, P < 0.001) (Supplementary Figures S7G, I).

Construction and validation of the nomogram

We also constructed a nomogram for predicting patients' prognosis. We performed univariate and multivariate Cox regression analyses of various clinical characteristics (age and TNM stage) to assess whether the risk score could serve as an independent prognostic factor. Regardless of the type of Cox regression analysis that was performed, the risk score consistently showed high prognostic value (Figs. 8A and B). Additionally, a nomogram was generated by using multivariate Cox regression analysis, which further demonstrated the significant ability of the risk score to predict clinical outcomes (Fig. 8C). We also utilized ROC curves to evaluate the effectiveness of the nomogram for predicting patient prognosis. The AUC values for 3-, 5-, and 10-year OS were 0.727, 0.622, and 0.672, respectively (Fig. 8D).

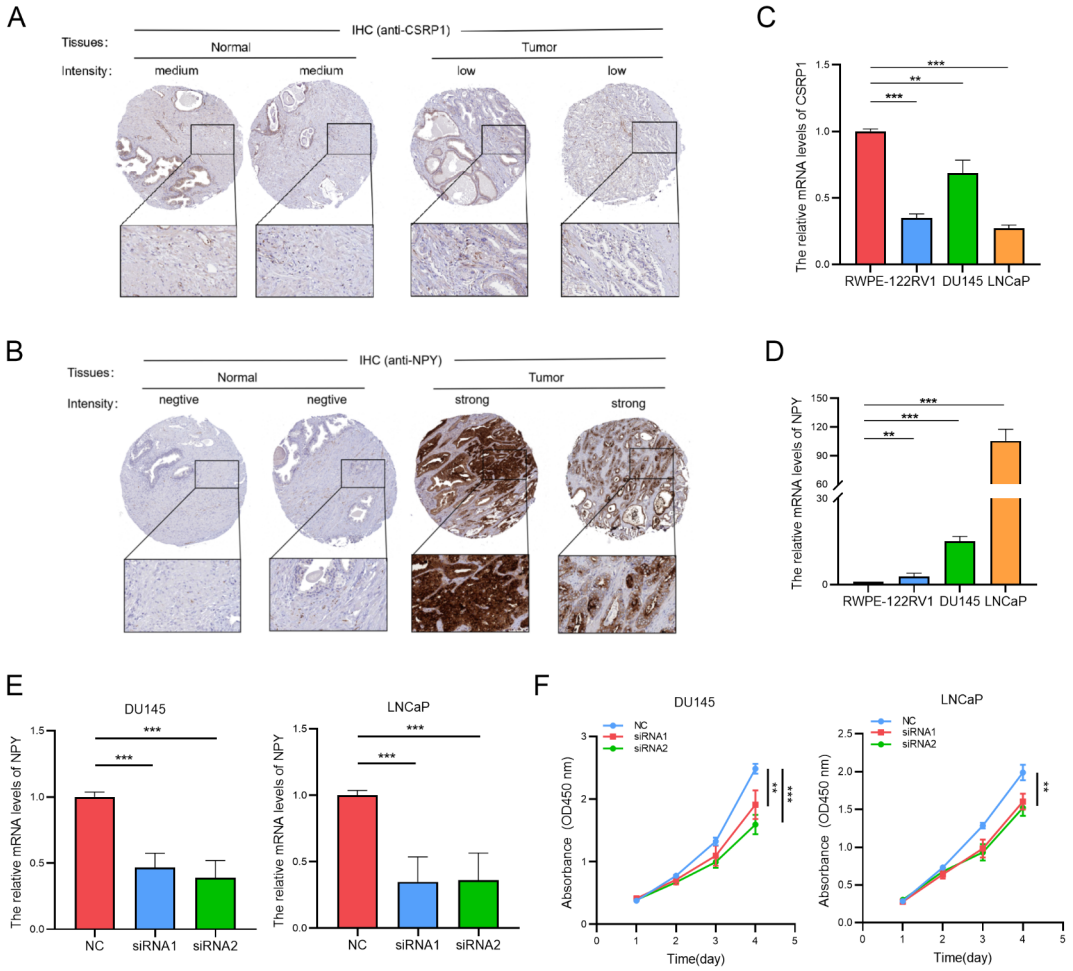

Fig. 7. The important role of key genes in PCa. (**A**-**B**) Protein expression levels of CSRP1 and NPY in normal and cancer tissues. (**C**-**D**) Comparison of the mRNA expression levels of CSRP1 and NPY between normal and cancer cell lines. (**E**) NPY mRNA expression levels after transfection with NPY-siRNAs in DU145 and LNCaP cell lines. (**F**) The proliferation ability of DU145 and LNCaP cell lines transfected with NPY-siRNAs.

TMB and drug susceptibility analysis

The success of immunotherapy relies heavily on the TMB[31]. To determine the most frequently mutated genes in PCa, we evaluated specific gene mutations. Our results demonstrated that TP53 had the highest mutation frequency in both groups, followed by SPOP (Supplementary Figures S8A and B). Additionally, we analysed somatic mutations associated with PCa and found that high-risk patients had a significantly greater TMB than low-risk patients did (Supplementary Figure S8C). To further investigate the potential of our findings, we examined whether the risk score could accurately predict the chemotherapy sensitivity of PCa patients. We examined the clinical efficacy of staurosporine, vorinostat, GNE-317, dasatinib, buparlisib, and pictilisib for PCa treatment. Our findings suggest that patients with a low risk score may exhibit greater sensitivity to staurosporine, dasatinib, GNE-317 (a PI3K/mTOR inhibitor), buparlisib (a PI3K inhibitor), and pictilisib (a PI3K inhibitor), thus indicating that chemotherapy is a promising option for patients in the low risk score group (Supplementary Figures S8D-I).

Discussion

PCa is a prevalent and lethal urinary malignancy affecting men worldwide[32]. Although early-stage PCa may not present with noticeable symptoms, advanced-stage disease often involves metastasis to lymph nodes and bones[33]. Consequently, there is a pressing need to identify and validate novel prognostic biomarkers to improve clinical therapeutic approaches and patient outcomes. ScRNA-seq has emerged as a valuable technique for investigating the heterogeneity and intercellular communication within various cancers, including PCa[34]. Hence, we propose a risk model that is based on a thorough examination of bulk RNA-seq and scRNA-seq data. This model has the potential to predict the prognosis of PCa patients and ascertain the advantages of immunotherapy and chemotherapy.

We obtained raw single-cell data from the GEO database, which consisted of 18 tumour samples, 14 adjacent cancer samples, and 5 normal samples. Our analysis used scRNA-seq to identify clinically relevant

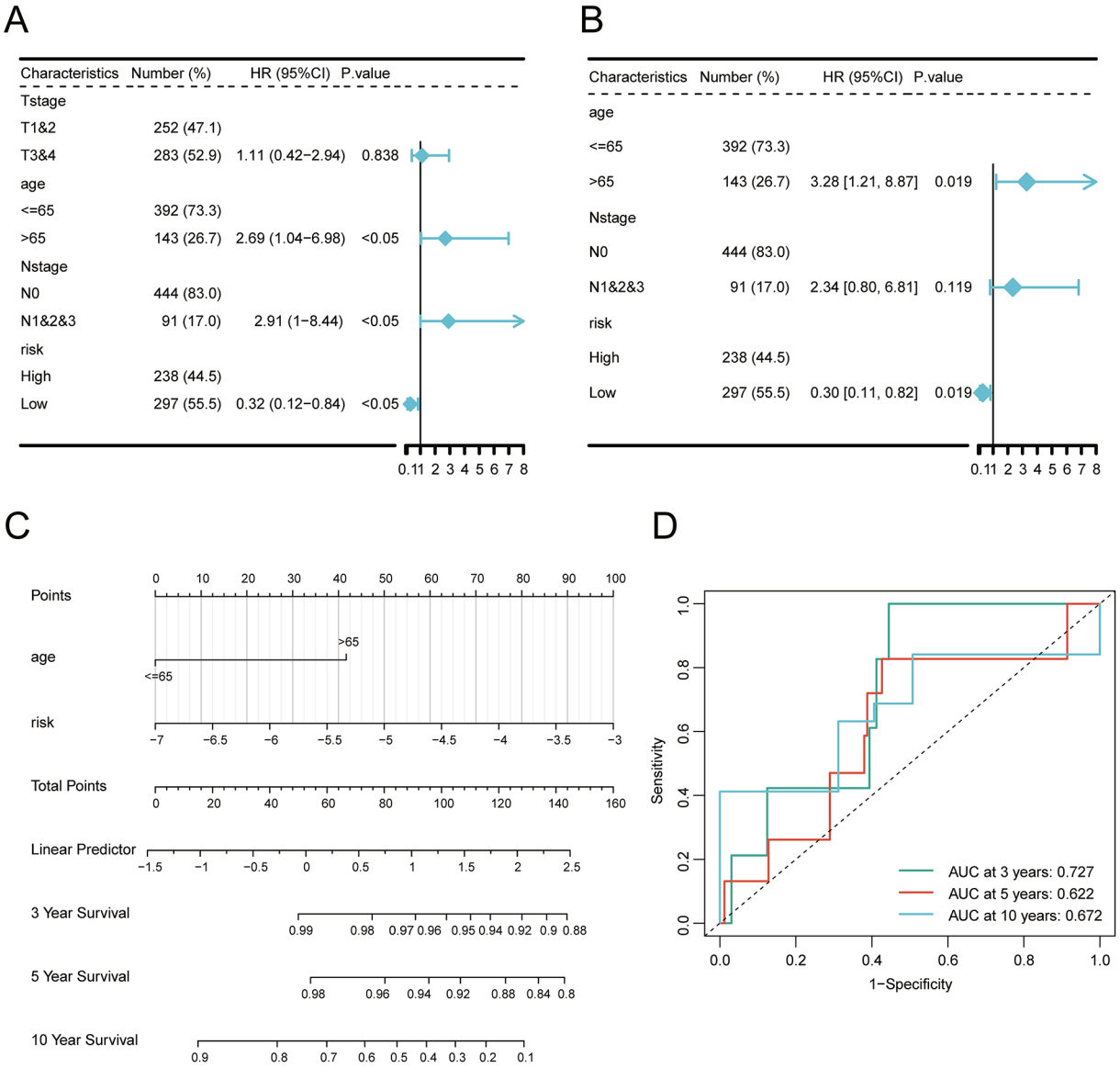

Fig. 8. Nomogram constructed with the risk score and clinical features. (**A**-**B**) Forest plot showing the results of univariate and multivariate Cox regression analyses of risk scores and clinical characteristics. (**C**) Nomogram based on clinicopathologic data and the risk score. (**D**) The time-dependent ROC curves of the nomogram model for the 3-, 5- and 10-year OS of patients.

microenvironments and cancer characteristics. In total, we obtained 147,856 cells. Fifteen cell types, including CTL, Treg, Thelper, mDC, and epithelial cells, were identified. Malignant tumour cells display increased activity of telomerase, which is an enzyme that is responsible for preserving telomere length in tumour cells, thus enabling unrestricted proliferation[35]. Consequently, we evaluated the expression patterns of TR genes to determine high TR gene scores at the single-cell level, it was found that highly active telomerase cells were mainly concentrated in mDC. Cell-cell communication analysis and pseudotime analysis based on mDCs further demonstrate their important role in PCa progression and suggest that mDCs promote the occurrence of PCa by affecting MHC-I and MIF pathways.

DCs play a critical role in tumour development by influencing T-cell immunity through induction, regulation, and maintenance[36]. Additionally, DCs contribute to immune tolerance by promoting T-cell deletion, unresponsiveness, as well as activation of regulatory T cells[9]. The TME in PCa patients shows a notable increase in cell-cell communication interactions, with higher frequency and intensity compared to normal tissue. Notably, most interactions among immune cells also exhibit heightened quantity and strength. This complex interplay and inherent heterogeneity within the TME are essential factors in tumour progression and the development of drug resistance[37]. Afterwards, we integrated data from single-cell and transcriptome sequencing to identify the core genes that affect PCa progression among TR genes. By intersecting the differential genes between mDCs and all other cells with all the differential genes affecting PCa progression, we obtained 249 hub genes. In addition, the results of functional enrichment analysis demonstrated that the DEGs associated

with telomeres in PCa were enriched in crucial immune system processes, including Th17 cell differentiation, Th1 and Th2 cell differentiation, and antigen processing. Th17 cells play a critical role in adaptive immunity, thus assisting the host in defending against extracellular pathogens[38–40]. In addition to their contributions to antitumour immunity and anti-aging resistance, TRDEGs also play a significant role in autoimmune-mediated inflammatory diseases. These findings suggest that these DEGs related to telomeres induce the development of PCa by affecting the normal function of the immune system. Subsequently, we compared the DEGs between PCa tissues and adjacent tissues with the TRDEGs. We conducted univariate Cox analysis of the resulting 249 candidate genes related to PCa and ultimately identified 7 genes that are associated with PCa prognosis.

Based on the 7 prognosis-related genes, we used the LASSO algorithm to screen and obtained 2 hub genes (CSRP1 and NPY). We then constructed a prognostic model including CSRP1 and NPY genes. To validate the model, the mRNA expression levels were determined. The qRT-PCR results were obtained from prostate cells (RWPE-1) and tumour cell lines (22RV1, DU145, and LNCaP). The findings demonstrated a marked increase in NPY expression in the tumour cell lines, whereas the expression pattern of CSRP1 exhibited the opposite trend. In addition, cell viability was significantly decreased when NPY was knocked down in LNCaP and DU145 cells, confirming the important role of NPY and CSRP1 in PCa progression. The results of the ROC curve analysis showed that the model performed well in predicting patient prognosis at 3, 5, and 10 years, with AUC values ranging from 0.706 to 0.974. This finding was further supported by the validation set, in which the AUC was between 0.672 and 0.886, thus indicating increased reliability and relevance of the model. Moreover, our signature, which is the result of integrating multiple datasets and algorithms, consists of only two genes and has a relatively simple scoring system when compared to other models. Studies have shown that CSRP1 is aberrantly expressed in malignant tumours. For instance, an anticancer role for CSRP1 has been demonstrated in hepatocellular carcinoma[41]. Inhibition of xenograft growth was observed in cells with low CSRP1 expression, thus suggesting that CSRP1 is a new independent prognostic factor for COAD[42]. Conversely, breast cancer has been associated with increased expression of CSRP1, thus indicating its potential as a carcinogen. This effect may be attributed to RNA binding dysfunction[43]. Neuropeptide Y (NPY) has been found to promote tumour cell growth, migration, metastasis, and angiogenesis[44,45]. Similarly, NPY has also been proven to affect the proliferation and migration of breast cancer cells[46,47]. In the context of renal cell carcinoma, NPY regulates the p53-dependent apoptotic pathway through Y1R, thus leading to a reduction in the expression of proapoptotic proteins[48]. This consequently affects the cytotoxicity of cisplatin to cancer cells. Similar effects have been observed in neuroblastoma, wherein NPY enhances cell viability by exerting antiapoptotic effects and attenuating endoplasmic reticulum stress[49]. Our research findings support this supposition, as we observed that the downregulation of NPY expression effectively inhibited the proliferation of LNCap and DU145 cells. However, it is worth noting that NPY can play an antitumour role in certain other cancers, such as liver cancer[50].

We also investigated the relationship between high- and low-risk groups and the TME, which plays a crucial role in cancer progression[51]. An understanding of the immune cells that are present in the TME can potentially advance immunotherapy. This study aimed to examine the differences in immune cell infiltration between two groups of patients with different risk models, when considering that the TME not only impacts cancer prognosis but also affects the effectiveness of anticancer therapies. The results demonstrated significant differences in the infiltration of various immune cells, including activated CD4 + T cells, central memory cells, and CD4 + T cells, between the high- and low-risk groups. CD4 + T cells have been increasingly recognized for their vital role in cancer immunity, and a separate study on PCa highlighted the association between CD4 + and CD8 + T-cells infiltration and tumour growth[52,53]. Monocytes and proinflammatory macrophages derived from monocytes generally play crucial roles in the pathogenesis of common diseases, such as infectious diseases, obesity, cancer, Alzheimer's disease, and atherosclerosis. A greater proportion of monocytes infiltrating the tumour environment indicates a poor clinical prognosis for cancer patients[54,55]. TMB is a key factor in the success of immunotherapy, and the analysis of somatic cell mutations associated with PCa demonstrated that the TMB was significantly greater in the high-risk group than in the low-risk group[31]. Thus, we propose that the risk score may be used as a potential predictive tool for immunotherapy patients.

We also conducted univariate and multivariate Cox regression analyses to examine the associations between the risk models and clinicopathological features. Our findings demonstrated the significant independent prognostic significance of the risk score for patients. To visually demonstrate the predictive ability of the risk score, we created a nomogram showing its significant correlation with clinical outcomes. Moreover, by using the GDSC database, we evaluated the ability of the model to predict chemosensitivity in PCa patients. Our results suggest that patients with low-risk scores may exhibit increased sensitivity to dasatinib, PI3K pathway inhibitors, and cell cycle inhibitors. Chemotherapy appears to be a promising treatment option for these patients. Notably, dasatinib, which is a drug that is currently used in the clinical treatment of leukaemia, holds a significant position in tumour chemotherapy research and has potential as an effective antitumour drug in the future[56]. However, it is crucial to acknowledge some limitations inherent in this study. Firstly, the prognostic model was formulated based on publicly available datasets, thus necessitating additional validation through extensive prospective clinical studies to ascertain its predictive accuracy. Secondly, comprehensive and detailed investigations are required to substantiate the mechanisms by which the prognostic genes influence PCa.

Conclusion

In this study, we conducted bioinformatics analysis using scRNA-seq and bulk RNA-seq data and found that TR genes are mainly concentrated in the mDCs of PCa patients, affecting disease progression through MIF and MHC-I. Further analysis revealed seven key prognostic genes and allowed us to construct a prognostic model specific to PCa. ROC analysis and cellular experiments confirmed the predictive role of hub genes and the model in PCa. These studies provide an in-depth analysis and novel targets for the role of TR genes in the clinical

progression of PCa patients, offering new insights into the diagnosis and clinical treatment of PCa patients and potentially contributing to improving clinical outcomes for patients.

Data availability

The datasets that were used and/or analysed during the current study are available from TCGA (https://portal.gdc.cancer.gov/) and GEO (https://www.ncbi.nlm.nih.gov/geo/).

Received: 29 July 2024; Accepted: 14 April 2025
Published online: 25 April 2025

References

1. Han, K. et al. Luteolin inhibited proliferation and induced apoptosis of prostate cancer cells through miR-301. *Onco Targets Ther.* **9**, 3085–3094. https://doi.org/10.2147/OTT.S102862 (2016).
2. Siegel, R. L., Miller, K. D., Wagle, N. S. & Jemal, A. Cancer statistics, 2023. *CA Cancer J. Clin.* **73**, 17–48. https://doi.org/10.3322/caac.21763 (2023).
3. Xie, M. et al. RK-33 radiosensitizes prostate Cancer cells by blocking the RNA helicase DDX3. *Cancer Res.* **76**, 6340–6350. https://doi.org/10.1158/0008-5472.CAN-16-0440 (2016).
4. Kulkarni, A. S., Gubbi, S. & Barzilai, N. Benefits of Metformin in attenuating the hallmarks of aging. *Cell. Metab.* **32**, 15–30. https://doi.org/10.1016/j.cmet.2020.04.001 (2020).
5. Zhao, Z. et al. Cascaded electrochemiluminescence signal amplifier for the detection of telomerase activity from tumor cells and tissues. *Theranostics* **8**, 5625–5633. https://doi.org/10.7150/thno.27680 (2018).
6. Clynes, D. et al. Suppression of the alternative lengthening of telomere pathway by the chromatin remodelling factor ATRX. *Nat. Commun.* **6**, 7538. https://doi.org/10.1038/ncomms8538 (2015).
7. Lanna, A. et al. An intercellular transfer of telomeres rescues T cells from senescence and promotes long-term immunological memory. *Nat. Cell. Biol.* **24**, 1461–1474. https://doi.org/10.1038/s41556-022-00991-z (2022).
8. Pardi, N., Hogan, M. J., Porter, F. W. & Weissman, D. mRNA vaccines - a new era in vaccinology. *Nat. Rev. Drug Discov.* **17**, 261–279. https://doi.org/10.1038/nrd.2017.243 (2018).
9. Palucka, K., Ueno, H., Fay, J. & Banchereau, J. Dendritic cells and immunity against cancer. *J. Intern. Med.* **269**, 64–73. https://doi.org/10.1111/j.1365-2796.2010.02317.x (2011).
10. Alkhateeb, A. et al. Transcriptomics signature from Next-Generation sequencing data reveals new transcriptomic biomarkers related to prostate Cancer. *Cancer Inf.* **18**, 1176935119835522. https://doi.org/10.1177/1176935119835522 (2019).
11. Want, M. Y. et al. WHSC1/NSD2 regulates immune infiltration in prostate cancer. *J. Immunother Cancer.* **9** https://doi.org/10.1136/jitc-2020-001374 (2021).
12. Hamzeh, O. et al. A hierarchical machine learning model to discover Gleason Grade-Specific biomarkers in prostate Cancer. *Diagnostics (Basel).* **9** https://doi.org/10.3390/diagnostics9040219 (2019).
13. Butler, A., Hoffman, P., Smibert, P., Papalexi, E. & Satija, R. Integrating single-cell transcriptomic data across different conditions, technologies, and species. *Nat. Biotechnol.* **36**, 411–420. https://doi.org/10.1038/nbt.4096 (2018).
14. Qiu, X. et al. Reversed graph embedding resolves complex single-cell trajectories. *Nat. Methods.* **14**, 979–982. https://doi.org/10.1038/nmeth.4402 (2017).
15. Karmaus, P. W. F. et al. Metabolic heterogeneity underlies reciprocal fates of T(H)17 cell stemness and plasticity. *Nature* **565**, 101–105. https://doi.org/10.1038/s41586-018-0806-7 (2019).
16. Fang, Z. et al. Single-Cell transcriptomics of proliferative phase endometrium: systems analysis of Cell-Cell communication network using cellchat. *Front. Cell. Dev. Biol.* **10**, 919731. https://doi.org/10.3389/fcell.2022.919731 (2022).
17. Gene Ontology, C. Gene ontology consortium: going forward. *Nucleic Acids Res.* **43**, D1049–1056. https://doi.org/10.1093/nar/gku1179 (2015).
18. Kanehisa, M. & Goto, S. KEGG: Kyoto encyclopedia of genes and genomes. *Nucleic Acids Res.* **28**, 27–30. https://doi.org/10.1093/nar/28.1.27 (2000).
19. Yu, G., Wang, L. G., Han, Y. & He, Q. Y. ClusterProfiler: an R package for comparing biological themes among gene clusters. *OMICS* **16**, 284–287. https://doi.org/10.1089/omi.2011.0118 (2012).
20. Kanehisa, M. Toward Understanding the origin and evolution of cellular organisms. *Protein Sci.* **28**, 1947–1951. https://doi.org/10.1002/pro.3715 (2019).
21. Kanehisa, M., Furumichi, M., Sato, Y., Kawashima, M. & Ishiguro-Watanabe, M. KEGG for taxonomy-based analysis of pathways and genomes. *Nucleic Acids Res.* **51**, D587–D592. https://doi.org/10.1093/nar/gkac963 (2023).
22. Friedman, J., Hastie, T. & Tibshirani, R. Regularization paths for generalized linear models via coordinate descent. *J. Stat. Softw.* **33**, 1–22 (2010).
23. Subramanian, A. et al. Gene set enrichment analysis: a knowledge-based approach for interpreting genome-wide expression profiles. *Proc. Natl. Acad. Sci. U S A.* **102**, 15545–15550. https://doi.org/10.1073/pnas.0506580102 (2005).
24. Liberzon, A. et al. Molecular signatures database (MSigDB) 3.0. *Bioinformatics* **27**, 1739–1740. https://doi.org/10.1093/bioinformatics/btr260 (2011).
25. Wu, S. et al. Integrated machine learning and Single-Sample gene set enrichment analysis identifies a TGF-Beta signaling pathway derived score in headneck squamous cell carcinoma. *J. Oncol.* **2022** (3140263). https://doi.org/10.1155/2022/3140263 (2022).
26. Ru, B. et al. TISIDB: an integrated repository portal for tumor-immune system interactions. *Bioinformatics* **35**, 4200–4202. https://doi.org/10.1093/bioinformatics/btz210 (2019).
27. Mayakonda, A., Lin, D. C., Assenov, Y., Plass, C. & Koeffler, H. P. Maftools: efficient and comprehensive analysis of somatic variants in cancer. *Genome Res.* **28**, 1747–1756. https://doi.org/10.1101/gr.239244.118 (2018).
28. Liu, Z. et al. TTN/OBSCN 'Double-Hit' predicts favourable prognosis, 'immune-hot' subtype and potentially better immunotherapeutic efficacy in colorectal cancer. *J. Cell. Mol. Med.* **25**, 3239–3251. https://doi.org/10.1111/jcmm.16393 (2021).
29. Yang, W. et al. Genomics of drug sensitivity in Cancer (GDSC): a resource for therapeutic biomarker discovery in cancer cells. *Nucleic Acids Res.* **41**, D955–961. https://doi.org/10.1093/nar/gks1111 (2013).
30. Maeser, D., Gruener, R. F. & Huang, R. S. OncoPredict: an R package for predicting in vivo or cancer patient drug response and biomarkers from cell line screening data. *Brief. Bioinform.* **22** https://doi.org/10.1093/bib/bbab260 (2021).
31. Song, W. et al. Synergistic and low adverse effect cancer immunotherapy by Immunogenic chemotherapy and locally expressed PD-L1 trap. *Nat. Commun.* **9**, 2237. https://doi.org/10.1038/s41467-018-04605-x (2018).
32. Tsui, K. H. et al. The inhibitory effects of capillarisin on cell proliferation and invasion of prostate carcinoma cells. *Cell. Prolif.* **51**, e12429. https://doi.org/10.1111/cpr.12429 (2018).
33. Lian, H., Wu, J., Hu, Y. & Guo, H. Self-assembled albumin nanoparticles for combination therapy in prostate cancer. *Int. J. Nanomed.* **12**, 7777–7787. https://doi.org/10.2147/IJN.S144634 (2017).
34. Serin Harmanci, A., Harmanci, A. O. & Zhou, X. CaSpER identifies and visualizes CNV events by integrative analysis of single-cell or bulk RNA-sequencing data. *Nat. Commun.* **11**, 89. https://doi.org/10.1038/s41467-019-13779-x (2020).

35. Kim, J. Y. et al. Alternative lengthening of telomeres in primary pancreatic neuroendocrine tumors is associated with aggressive clinical behavior and poor survival. *Clin. Cancer Res.* **23**, 1598–1606. https://doi.org/10.1158/1078-0432.CCR-16-1147 (2017).
36. Wang, Y. et al. LKB1 orchestrates dendritic cell metabolic quiescence and anti-tumor immunity. *Cell. Res.* **29**, 391–405. https://doi.org/10.1038/s41422-019-0157-4 (2019).
37. Lee, H. W. et al. Single-cell RNA sequencing reveals the tumor microenvironment and facilitates strategic choices to circumvent treatment failure in a chemorefractory bladder cancer patient. *Genome Med.* **12**, 47. https://doi.org/10.1186/s13073-020-00741-6 (2020).
38. Xu, H. et al. The induction and function of the anti-inflammatory fate of T(H)17 cells. *Nat. Commun.* **11**, 3334. https://doi.org/10.1038/s41467-020-17097-5 (2020).
39. Zhao, Z. et al. The PRAK-NRF2 axis promotes the differentiation of Th17 cells by mediating the redox homeostasis and Glycolysis. *Proc. Natl. Acad. Sci. U S A.* **120**, e2212613120. https://doi.org/10.1073/pnas.2212613120 (2023).
40. Block, M. S. et al. Th17-inducing autologous dendritic cell vaccination promotes antigen-specific cellular and humoral immunity in ovarian cancer patients. *Nat. Commun.* **11**, 5173. https://doi.org/10.1038/s41467-020-18962-z (2020).
41. Hirasawa, Y. et al. Methylation status of genes upregulated by demethylating agent 5-aza-2'-deoxycytidine in hepatocellular carcinoma. *Oncology* **71**, 77–85. https://doi.org/10.1159/000100475 (2006).
42. Yu, S. et al. CSRP1 promotes Colon adenocarcinoma growth and serves as an independent risk biomarker for worse prognosis. *Genet. Res. (Camb).* **2023** (8586507). https://doi.org/10.1155/2023/8586507 (2023).
43. Lopez-Cortes, A. et al. Prediction of breast cancer proteins involved in immunotherapy, metastasis, and RNA-binding using molecular descriptors and artificial neural networks. *Sci. Rep.* **10**, 8515. https://doi.org/10.1038/s41598-020-65584-y (2020).
44. Yang, Z. et al. Structural basis of ligand binding modes at the neuropeptide Y Y(1) receptor. *Nature* **556**, 520–524. https://doi.org/10.1038/s41586-018-0046-x (2018).
45. Czarnecka, M. et al. Neuropeptide Y receptor interactions regulate its mitogenic activity. *Neuropeptides* **73**, 11–24. https://doi.org/10.1016/j.npep.2018.11.008 (2019).
46. Medeiros, P. J. et al. Neuropeptide Y stimulates proliferation and migration in the 4T1 breast cancer cell line. *Int. J. Cancer.* **131**, 276–286. https://doi.org/10.1002/ijc.26350 (2012).
47. Wang, Y. et al. A Y(1) receptor ligand synergized with a P-glycoprotein inhibitor improves the therapeutic efficacy of multidrug resistant breast cancer. *Biomater. Sci.* **7**, 4748–4757. https://doi.org/10.1039/c9bm00337a (2019).
48. Kim, N. et al. Neuropeptide Y protects kidney against cisplatin-induced nephrotoxicity by regulating p53-dependent apoptosis pathway. *BMB Rep.* **49**, 288–292. https://doi.org/10.5483/bmbrep.2016.49.5.231 (2016).
49. Palanivel, V. et al. Neuroprotective Effects of Neuropeptide Y on Human Neuroblastoma SH-SY5Y Cells in Glutamate Excitotoxicity and ER Stress Conditions. *Cells* 11, (2022). https://doi.org/10.3390/cells11223665
50. Levite, M., Safadi, R., Milgrom, Y., Massarwa, M. & Galun, E. Neurotransmitters and neuropeptides decrease PD-1 in T cells of healthy subjects and patients with hepatocellular carcinoma (HCC), and increase their proliferation and eradication of HCC cells. *Neuropeptides* **89**, 102159. https://doi.org/10.1016/j.npep.2021.102159 (2021).
51. Zhang, M. et al. Adipocyte-Derived lipids mediate melanoma progression via FATP proteins. *Cancer Discov.* **8**, 1006–1025. https://doi.org/10.1158/2159-8290.CD-17-1371 (2018).
52. Morris, E. C. & Stauss, H. J. Optimizing T-cell receptor gene therapy for hematologic malignancies. *Blood* **127**, 3305–3311. https://doi.org/10.1182/blood-2015-11-629071 (2016).
53. Strasner, A. & Karin, M. Immune infiltration and prostate Cancer. *Front. Oncol.* **5**, 128. https://doi.org/10.3389/fonc.2015.00128 (2015).
54. Sharma, S. et al. APOBEC3A cytidine deaminase induces RNA editing in monocytes and macrophages. *Nat. Commun.* **6**, 6881. https://doi.org/10.1038/ncomms7881 (2015).
55. Jeong, J., Suh, Y. & Jung, K. Context drives diversification of monocytes and neutrophils in orchestrating the tumor microenvironment. *Front. Immunol.* **10**, 1817. https://doi.org/10.3389/fimmu.2019.01817 (2019).
56. Chen, R. et al. Evolution of genomic and T-cell repertoire heterogeneity of malignant pleural mesothelioma under dasatinib treatment. *Clin. Cancer Res.* **26**, 5477–5486. https://doi.org/10.1158/1078-0432.CCR-20-1767 (2020).

Acknowledgements

We would like to acknowledge the Engineering Laboratory of Urinary Organ and Functional Reconstruction of Shandong Provincial Hospital for supporting. Figure1 was completed using Figdraw.

Author contributions

Danfeng Zhao and Qiang Fu designed the research; Zhenjie Zang performed the experiments; Danfeng Zhao, Guanbo Wang and Haodong Li analysed the data; Danfeng Zhao, Ruiyu Li and Keqin Zhang wrote the manuscript; Qiang Fu and Tongxiang Diao edited the manuscript. All of the authors have read and approved the final manuscript.

Funding

This study was supported by the National Key Research and Development Program of China (Grant numbers: 2021YFC2009300 and 2021YFC2009304), the National Natural Science Foundation of China (Grant numbers: 82071635 and 81873830), and the Shandong Provincial Natural Science Foundation (ZR2021QH366).

Declarations

Competing interests

The authors declare no competing interests.

Additional information

Supplementary Information The online version contains supplementary material available at https://doi.org/10.1038/s41598-025-98663-z.

Correspondence and requests for materials should be addressed to Q.F.